

Bound-preserving and entropy stable enriched Galerkin methods for nonlinear hyperbolic equations

Dmitri Kuzmin^a, Sanghyun Lee^b, Yi-Yung Yang^b

^a*Institute of Applied Mathematics, TU Dortmund University, Vogelpothsweg 87, Dortmund, D-44227, Germany*

^b*Department of Mathematics, Florida State University, 1017 Academic Way, Tallahassee, 32306-4510, FL, USA*

Abstract

In this paper, we develop monolithic limiting techniques for enforcing nonlinear stability constraints in enriched Galerkin (EG) discretizations of nonlinear scalar hyperbolic equations. To achieve local mass conservation and gain control over the cell averages, the space of continuous (multi-)linear finite element approximations is enriched with piecewise-constant functions. The resulting spatial semi-discretization has the structure of a variational multiscale method. For linear advection equations, it is inherently stable but generally not bound preserving. To satisfy discrete maximum principles and ensure entropy stability in the nonlinear case, we use limiters adapted to the structure of our locally conservative EG method. The cell averages are constrained using a flux limiter, while the nodal values of the continuous component are constrained using a clip-and-scale limiting strategy for antidiffusive element contributions. The design and analysis of our new algorithms build on recent advances in the fields of convex limiting and algebraic entropy fixes for finite element methods. In addition to proving the claimed properties of the proposed approach, we conduct numerical studies for two-dimensional nonlinear hyperbolic problems. The numerical results demonstrate the ability of our limiters to prevent violations of the imposed constraints, while preserving the optimal order of accuracy in experiments with smooth solutions.

Keywords:

nonlinear hyperbolic conservation laws, finite elements, enriched Galerkin method, discrete maximum principles, entropy stability, algebraic flux correction, convex limiting

1. Introduction

Hyperbolic problems find extensive applications across various fields, playing a crucial role in understanding phenomena such as aquifer contaminant transport [1], shallow water dynamics [2, 3], petroleum engineering for oil and gas production [4, 5, 6], and environmental engineering [7, 8]. The evolution equations that model various transport phenomena are typically derived from fundamental physical laws, such as conservation principles. Since exact weak solutions of nonlinear hyperbolic problems can be discontinuous and nonunique (even for smooth initial data), computation of physically admissible numerical solutions presents significant challenges. A well-designed discretization method should be sufficiently dissipative to prevent spurious oscillations, nonphysical states and convergence to wrong weak solutions. On the other hand, the levels of numerical viscosity should be kept as low as possible to achieve high resolution.

The framework of algebraic flux correction (AFC) [9, 10, 11] makes it possible to incorporate appropriate constraints, such as discrete conservation/maximum principles and entropy inequalities, into finite element discretizations of scalar conservation laws and hyperbolic systems. Splitting a high-order discretization into a property-preserving low-order part and an antidiffusive remainder, AFC schemes constrain the latter in an adaptive and conservative manner. Examples of such nonlinear stabilization techniques include various generalizations [12, 13, 14] of Zalesak’s flux-corrected transport (FCT) algorithm [15]. The element-based FCT schemes introduced in [16, 17] in the context of linear advection problems use convex decompositions to keep the nodal values of finite element approximations in the admissible range under local constraints that are easy to enforce using limiters. For nonlinear hyperbolic systems, an edge-based FCT algorithm of this kind was proposed by Guermond et al. [18], who used it to enforce preservation of invariant domains, i.e., of convex admissible sets containing all possible states of exact solutions. The monolithic convex limiting (MCL) strategy introduced in [19] makes it possible to constrain spatial semi-discretizations instead of fully discrete schemes. In contrast to FCT-like predictor-corrector algorithms, MCL discretizations have well-defined residuals and steady-state solutions. Moreover, they can be equipped with limiter-based entropy fixes [20, 21] based on Tadmor’s entropy stability theory [22]. A comprehensive review of the state of the art in the design and analysis of limiting techniques for finite elements can be found in [23].

In the literature on AFC schemes, discretization in space is typically performed using a continuous Galerkin (CG) or discontinuous Galerkin (DG) method. The advantages of DG approximations include the local conservation property and optimal convergence behavior for linear hyperbolic problems with smooth solutions. However, the number of degrees of freedom is considerably greater than that for a CG approximation using finite elements of the same polynomial degree. As an attractive alternative, we consider an enriched Galerkin (EG) method¹ [25, 26, 27], in which a discontinuous \mathbb{P}_0 component δu_h is added to the continuous \mathbb{P}_1 or \mathbb{Q}_1 component u_h of the numerical solution $u_h^{\text{EG}} = u_h + \delta u_h$. The EG formulation can be interpreted as a variational multiscale method in which the evolution equation for δu_h serves as a subgrid scale model [28]. The favorable properties of the DG- \mathbb{P}_1 method are achieved at a lower cost, because the EG version uses less degrees of freedom and produces linear systems that can be solved efficiently [26]. Moreover, the local mass conservation property of EG has been exploited in various applications including two-phase flow [29], poroelasticity [30, 31], and thermo-poroelasticity [32].

The first bound-preserving EG method for linear advection problems was designed in [33] using tailor-made limiters of FCT and MCL type for fluxes and element contributions. In the present paper, we extend the MCL version to nonlinear hyperbolic conservation laws in a manner that enables us to enforce entropy inequalities in addition to maximum principles. For the cell averages that define the DG component δu_h of u_h^{EG} , we use the flux limiting strategy proposed in [34]. Element contributions to the evolution equation for the CG component u_h are constrained using a clip-and-scale limiting algorithm, which we equip with a built-in entropy fix. Extensive numerical experiments demonstrate the ability of our method to produce physically consistent results while achieving optimal convergence rates. To the best of our knowledge, this is the first successful application of AFC tools to EG discretizations of nonlinear hyperbolic problems.

This paper is organized as follows. In Section 2, we formulate the continuous initial value problem and define the entropy solution, which represents a unique vanishing viscosity limit. In Section 3, we introduce a baseline EG discretization that features a group finite element (GFE)

¹In the original publication [24], the inventors of EG called it a reduced \mathbb{P}_1 -discontinuous Galerkin method.

approximation to the nonlinear flux function. In Section 4, we present the bound-preserving and entropy stable (but low-order accurate) local Lax–Friedrichs-type schemes for the cell averages and CG components of our finite element approximation. In Section 5, we define the limited antidiffusive terms that recover the high-order EG target in smooth regions, while preserving local bounds and maintaining entropy stability of the semi-discrete AFC scheme. In particular, we present and analyze our new entropic clip-and-scale limiter here. In Section 6, we discretize in time using an explicit strong stability preserving Runge–Kutta (SSP2/Heun) method. In Section 7, we conduct in-depth numerical studies for scalar nonlinear hyperbolic problems. For visualization purposes, we perform constrained L^2 projections of EG solutions into the CG space (as in [33]). Finally, the results are discussed and conclusions are drawn in Section 8.

2. Continuous problem

Let $u(\mathbf{x}, t) \in \mathbb{R}$ denote the value of a scalar conserved quantity u at a space location $\mathbf{x} \in \mathbb{R}^d$, $d \in \{1, 2, 3\}$ and time $t \geq 0$. We consider the initial value problem

$$\frac{\partial u}{\partial t} + \nabla \cdot \mathbf{f}(u) = 0 \quad \text{in } \Omega \times \mathbb{R}_+, \quad (1a)$$

$$u(\cdot, 0) = u_0 \quad \text{in } \Omega, \quad (1b)$$

where $\Omega \subset \mathbb{R}^d$ is a Lipschitz domain, $\mathbf{f}(u) := (f_1(u), \dots, f_d(u))$ is the flux function of the (possibly nonlinear) hyperbolic conservation law, and $u_0 : \Omega \rightarrow \mathbb{R}$ denotes the initial datum.

If periodic boundary conditions are imposed on $\partial\Omega$, the formulation (1) of the continuous problem is complete. In the non-periodic case, we prescribe the inflow boundary condition

$$u = u_{\text{in}}, \quad \text{on } \Gamma^{\text{in}} \times \mathbb{R}_+ \quad (2)$$

at the inlet $\Gamma^{\text{in}} := \{\mathbf{x} \in \partial\Omega : \mathbf{f}'(u) \cdot \mathbf{n} < 0\}$, where $\mathbf{f}'(u) = (f'_1(u), \dots, f'_d(u))$ is the flux Jacobian and \mathbf{n} is the unit outward normal to $\partial\Omega$. No boundary condition is imposed on $\Gamma^{\text{out}} := \partial\Omega \setminus \Gamma^{\text{in}}$.

Because of hyperbolicity, there exists a convex entropy $\eta(u)$ and an associated entropy flux $\mathbf{q}(u)$, i.e., a function $\mathbf{q} : \mathbb{R} \rightarrow \mathbb{R}^d$ of $\eta : \mathbb{R} \rightarrow \mathbb{R}$ such that $\mathbf{q}'(u) = \eta'(u)\mathbf{f}'(u)$. If problem (1) has a smooth classical solution u , the entropy conservation law

$$\frac{\partial \eta(u)}{\partial t} + \nabla \cdot \mathbf{q}(u) = 0 \quad \text{in } \Omega \times \mathbb{R}_+ \quad (3)$$

can be derived from (1a) using multiplication by the entropy variable $v(u) := \eta'(u)$, the chain rule, and the above definition of an entropy pair $\{\eta(u), \mathbf{q}(u)\}$. In general, the unique vanishing viscosity solution of (1) satisfies a weak form of the entropy inequality [22, 35]

$$\frac{\partial \eta(u)}{\partial t} + \nabla \cdot \mathbf{q}(u) \leq 0 \quad \text{in } \Omega \times \mathbb{R}_+ \quad (4)$$

for any entropy pair. Hence, entropy is conserved in smooth regions and dissipated at shocks.

3. High-order space discretization

Let $\mathcal{T}_h = \{K_e\}_{e=1}^{E_h}$ denote a non-degenerate partition of the domain Ω into E_h rectangular cells of maximum diameter $h = \max_{1 \leq e \leq E_h} h_{K_e}$, where h_{K_e} is the diameter of K_e . The vertices of \mathcal{T}_h are

denoted by $\mathbf{x}_1, \dots, \mathbf{x}_{N_h}$. We store the indices of vertices belonging to a given cell K_e in the integer set \mathcal{N}^e and the indices of elements that contain a given vertex \mathbf{x}_i in the integer set \mathcal{E}_i . The set $\mathcal{N}_i = \bigcup_{e \in \mathcal{E}_i} \mathcal{N}^e$ contains the indices of all vertices belonging to at least one cell that contains \mathbf{x}_i . Note that $i \in \mathcal{N}_i$. The boundary of a cell K_e consists of faces $S_{ee'}$ on which the outward normal $\mathbf{n}_{ee'}$ is constant. If $S_{ee'} = \partial K_e \cap \partial K_{e'}$ is an internal face, then $e' \in \{1, \dots, E_h\} \setminus \{e\}$ is the index of an adjacent cell $K_{e'}$. Boundary faces $S_{ee'} \subset \partial \Omega$ are associated with ∂E_h ghost cells and labeled using cell indices $e' \in \{E_h + 1, \dots, \bar{E}_h\}$, where $\bar{E}_h := E_h + \partial E_h$. We store the indices of faces of a cell K_e in the set \mathcal{Z}_e such that $\partial K_e = \bigcup_{e' \in \mathcal{Z}_e} S_{ee'}$. The unit outward normal to ∂K_e is denoted by \mathbf{n}_e if there is no ambiguity. See Figure 1 for a visual explanation of the above notation.

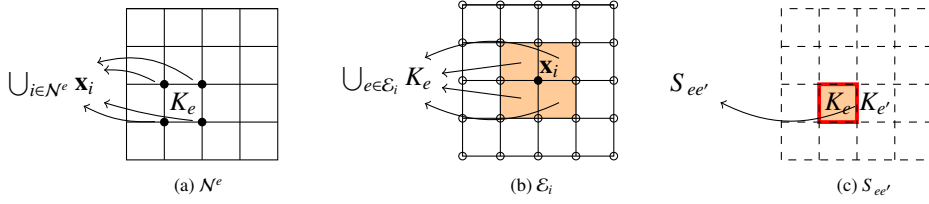


Figure 1: Visualization of the notation for vertices, cells, and faces of a uniform quadrilateral mesh.

3.1. Enriched Galerkin method

Let $\mathbb{Q}_1(\hat{K})$ denote the space of multilinear polynomials $\hat{v} : \hat{K} \rightarrow \mathbb{R}$ defined on the reference element $\hat{K} = [0, 1]^d$. Using a multilinear mapping $F_e : \hat{K} \rightarrow K_e \in \mathcal{T}_h$, we construct the space $\mathbb{Q}_1(K_e)$ of polynomials $v : K_e \rightarrow \mathbb{R}$ such that $v = \hat{v} \circ F_e^{-1}$ for some $\hat{v} \in \mathbb{Q}_1(\hat{K})$.

The finite element space CG- \mathbb{Q}_1 of the classical continuous Galerkin method using \mathbb{Q}_1 Lagrange elements on the partition \mathcal{T}_h is defined as

$$V_h^{\text{CG}} := \{v \in L^2(\Omega) : v|_{K_e} \in \mathbb{Q}_1(K_e) \forall K_e \in \mathcal{T}_h\} \cap \mathbb{C}(\bar{\Omega}),$$

where $\mathbb{C}(\bar{\Omega})$ denotes the space of functions that are continuous on $\bar{\Omega}$. The DG- \mathbb{Q}_0 space

$$V_h^{\text{DG}} := \{v \in L^2(\Omega) : v|_{K_e} \in \mathbb{Q}_0(K_e) \forall K_e \in \mathcal{T}_h\} \quad (5)$$

consists of functions that are constant on elements of the partition \mathcal{T}_h . As already mentioned in the introduction, we approximate exact weak solutions of (1) by

$$u_h^{\text{EG}} = u_h + \delta u_h \in V_h^{\text{CG}} \oplus V_h^{\text{DG}}, \quad (6)$$

where $u_h \in V_h^{\text{CG}}$ and $\delta u_h \in V_h^{\text{DG}}$. The space of such enriched Galerkin (EG- \mathbb{Q}_1) approximations (cf. [24, 33, 26, 27]) is denoted by V_h^{EG} . Figure 2 shows the local degrees of freedom (DOFs) for CG- \mathbb{Q}_1 , DG- \mathbb{Q}_0 , and EG- \mathbb{Q}_1 approximations on a patch consisting of four square cells.

Remark 1. We use quadrilateral meshes in this work but piecewise-linear (CG- \mathbb{P}_1) approximations u_h on triangles can be enriched by piecewise-constant functions $\delta u_h \in V_h^{\text{DG}}$ similarly. The linear stability analysis performed in [24] for EG discretizations of convection-diffusion equations is valid only for triangular meshes. However, the piecewise-constant enrichment of CG- \mathbb{Q}_1 approximations also provides the local conservation property and has a stabilizing effect.

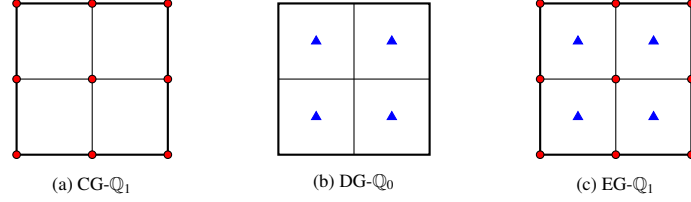


Figure 2: Degrees of freedom for finite element approximations on a patch of four cells.

The space V_h^{CG} is spanned by N_h global basis functions $\{\varphi_j\}_{j=1}^{N_h}$ such that $\varphi_j \in V_h^{\text{CG}}$ and $\varphi_j(\mathbf{x}_i) = \delta_{ij}$ for all $i, j \in \{1, \dots, N_h\}$. Hence, the CG component can be written as

$$u_h = \sum_{j=1}^{N_h} u_j \varphi_j \in V_h^{\text{CG}}, \quad (7)$$

where $u_j = u_h(\mathbf{x}_j)$ is the degree of freedom associated with φ_j . Similarly, the DG component

$$\delta u_h = \sum_{e=1}^{E_h} \delta u_e \chi_e \in V_h^{\text{DG}} \quad (8)$$

is defined by the coefficients δu_e of E_h characteristic functions χ_e such that $\chi_e = 1$ in K_e and $\chi_e = 0$ otherwise. The piecewise-constant basis functions χ_e span the space V_h^{DG} .

Using the EG method to discretize the nonlinear problem (1), we seek a numerical solution $u_h^{\text{EG}} \in V_h^{\text{EG}}$ that admits the decomposition (6) and satisfies the DG weak form [23]

$$\begin{aligned} \sum_{e=1}^{E_h} \int_{K_e} w_h^{\text{EG}} \frac{\partial u_h^{\text{EG}}}{\partial t} \, d\mathbf{x} + \sum_{e=1}^{E_h} \int_{\partial K_e} w_h^{\text{EG}} [\mathcal{F}(u_{h,e}^-, u_{h,e}^+; \mathbf{n}_e) - \mathbf{f}(u_{h,e}^{\text{EG}}) \cdot \mathbf{n}_e] \, ds \\ + \sum_{e=1}^{E_h} \int_{K_e} w_h^{\text{EG}} \nabla \cdot \mathbf{f}(u_h^{\text{EG}}) \, d\mathbf{x} = 0 \end{aligned} \quad (9)$$

of (1a) for all test functions $w_h^{\text{EG}} \in V_h^{\text{EG}}$. We define the local Lax-Friedrichs (LLF) flux

$$\mathcal{F}(u_L, u_R; \mathbf{n}) := \frac{\mathbf{f}(u_R) + \mathbf{f}(u_L)}{2} \cdot \mathbf{n} - \frac{\lambda_{LR}}{2} (u_R - u_L) \quad (10)$$

using the maximum wave speed [34]

$$\lambda_{LR} = \lambda_{\max}(u_L, u_R; \mathbf{n}) := \max_{\omega \in [0,1]} |\mathbf{f}'(\omega u_R + (1-\omega)u_L) \cdot \mathbf{n}|. \quad (11)$$

The internal and external states of the local Riemann problem are defined by

$$u_{h,e}^- = u_h + \delta u_e, \quad u_{h,e}^+ = \begin{cases} u_{\text{in}} & \text{on } \Gamma^{\text{in}}, \\ u_h + \delta u_e & \text{on } \Gamma^{\text{out}}, \\ u_h + \delta u_{e'} & \text{on } S_{ee'} = \partial K_e \cap \partial K_{e'}, \quad e' \leq E_h. \end{cases}$$

Integration by parts for the last term on the left-hand side of (9) yields

$$\sum_{e=1}^{E_h} \int_{K_e} w_h^{\text{EG}} \frac{\partial u_h^{\text{EG}}}{\partial t} \mathbf{d}\mathbf{x} + \sum_{e=1}^{E_h} \int_{\partial K_e} w_h^{\text{EG}} \mathcal{F}(u_{h,e}^-, u_{h,e}^+; \mathbf{n}_e) \mathbf{d}s - \sum_{e=1}^{E_h} \int_{K_e} \nabla w_h^{\text{EG}} \cdot \mathbf{f}(u_h^{\text{EG}}) \mathbf{d}\mathbf{x} = 0. \quad (12)$$

Any test function $w_h^{\text{EG}} \in V_h^{\text{EG}}$ can be written as $w_h^{\text{EG}} = w_h + \delta w_h$, where $w_h \in V_h^{\text{CG}}$ and $\delta w_h^{\text{EG}} \in V_h^{\text{DG}}$. In particular, w_h and δw_h are admissible test functions. Thus

$$\begin{aligned} \sum_{e=1}^{E_h} \int_{K_e} w_h \frac{\partial u_h^{\text{EG}}}{\partial t} \mathbf{d}\mathbf{x} + \sum_{e=1}^{E_h} \int_{\partial K_e \cap \partial \Omega} w_h \mathcal{F}(u_{h,e}^-, u_{h,e}^+; \mathbf{n}_e) \mathbf{d}s \\ - \sum_{e=1}^{E_h} \int_{K_e} \nabla w_h \cdot \mathbf{f}(u_h^{\text{EG}}) \mathbf{d}\mathbf{x} = 0 \quad \forall w_h \in V_h^{\text{CG}}, \end{aligned} \quad (13)$$

$$\sum_{e=1}^{E_h} \int_{K_e} \delta w_h \frac{\partial u_h^{\text{EG}}}{\partial t} \mathbf{d}\mathbf{x} + \sum_{e=1}^{E_h} \int_{\partial K_e} \delta w_h \mathcal{F}(u_{h,e}^-, u_{h,e}^+; \mathbf{n}_e) \mathbf{d}s = 0 \quad \forall \delta w_h \in V_h^{\text{DG}}. \quad (14)$$

Note that the surface integration in (13) is restricted to boundary faces of \mathcal{T}_h . The integrals over internal faces $S_{ee'} = \partial K_e \cap \partial K_{e'}$ cancel out for continuous test functions w_h .

As noticed by Becker et al. [24], the representation (6) of $u_h^{\text{EG}} \in V_h^{\text{EG}}$ is nonunique because any globally constant function can be represented exactly in V_h^{CG} and in V_h^{DG} alike. To ensure the uniqueness of δu_h defined by (8), we impose the additional constraint [33]

$$\delta u_e = \frac{1}{|K_e|} \int_{K_e} (u_h^{\text{EG}} - u_h) \mathbf{d}\mathbf{x} = U_e - \bar{u}_e, \quad e = 1, \dots, E_h, \quad (15)$$

where

$$U_e = \bar{u}_e = \frac{1}{|K_e|} \int_{K_e} u_h^{\text{EG}} \mathbf{d}\mathbf{x}, \quad \bar{u}_e = \frac{1}{|K_e|} \int_{K_e} u_h \mathbf{d}\mathbf{x}, \quad |K_e| = \int_{K_e} 1 \mathbf{d}\mathbf{x}. \quad (16)$$

In the remainder of this section, we derive evolution equations for the cell averages U_e of u_h^{EG} and the nodal values u_j of u_h defined by (7). The evolution of the DG component $\delta u_h = u_h^{\text{EG}} - u_h$ is then determined by our convention (15), which implies that δu_h is *massless* [33].

Remark 2. The analogy with variational multiscale methods for conservation laws (cf. [28]) makes it possible to interpret equations (14) and (15) as a subgrid scale model for δu_h .

3.2. High-order semi-discrete problem for EG cell averages

Using test functions $\delta w_h \in \{\chi_1, \dots, \chi_{E_h}\}$ in the semi-discrete weak form (14), we find that the cell averages of the EG solution u_h^{EG} must satisfy the local conservation laws

$$|K_e| \frac{\mathrm{d}U_e}{\mathrm{d}t} = - \int_{\partial K_e} \mathcal{F}(u_{h,e}^-, u_{h,e}^+; \mathbf{n}_e) \mathbf{d}s =: q_e^H, \quad e = 1, \dots, E_h, \quad (17)$$

where

$$u_{h,e}^- = u_h + (U_e - \bar{u}_e), \quad u_{h,e}^+ = \begin{cases} u_{\text{in}} & \text{on } \Gamma^{\text{in}}, \\ u_h + (U_e - \bar{u}_e) & \text{on } \Gamma^{\text{out}}, \\ u_h + (U_{e'} - \bar{u}_{e'}) & \text{on } S_{ee'} = \partial K_e \cap \partial K_{e'}, \quad e' \leq E_h. \end{cases}$$

The right-hand side q_e^H of equation (17) can be expressed in terms of the face-averaged fluxes

$$H_{ee'}^{\mathbb{Q}_1} = \frac{1}{|S_{ee'}|} \int_{S_{ee'}} \mathcal{F}(u_{h,e}^{\text{EG}}, u_{h,e'}^{\text{EG}}; \mathbf{n}_{ee'}) ds \quad (18)$$

as follows:

$$q_e^H = - \sum_{e' \in \mathcal{Z}_e} |S_{ee'}| H_{ee'}^{\mathbb{Q}_1}.$$

Throughout this paper, the superscript H refers to a ‘high-order’ approximation. The superscript L is reserved for the ‘low-order’ approximations to be presented in Section 4.

Let $\mathbf{U} = (U_e)_{e=1}^{E_h}$ denote the vector of EG cell averages and $\mathbf{q}^H = (q_e^H)_{e=1}^{E_h}$ the vector of discrete right-hand sides. By definition, $\mathbf{q}^H = \mathbf{q}^H(\mathbf{U}, \mathbf{u})$ depends not only on \mathbf{U} but also on the vector $\mathbf{u} = (u_i)_{i=1}^{N_h}$ of CG nodal values. Introducing the finite volume mass matrix $\bar{M} = \text{diag}(|K_e|)_{e=1}^{E_h}$, we write the system of ordinary differential equations (17) in the matrix form

$$\bar{M} \frac{d\mathbf{U}}{dt} = \mathbf{q}^H(\mathbf{U}, \mathbf{u}), \quad (19)$$

which will be referred to as the high-order (HO) semi-discrete problem for EG cell averages.

3.2.1. High-order semi-discrete problem for CG nodal values

Using the test functions $w_h^{\text{EG}} \in \{\varphi_1, \dots, \varphi_{N_h}\}$ in (9), we obtain the semi-discrete equations

$$\begin{aligned} \sum_{e \in \mathcal{E}} \int_{K_e} \varphi_i \frac{\partial u_h^{\text{EG}}}{\partial t} d\mathbf{x} + \sum_{e \in \mathcal{E}_i} \int_{\partial K_e \cap \partial \Omega} \varphi_i (\mathcal{F}(u_{h,e}^-, u_{h,e}^+; \mathbf{n}_e) - \mathbf{f}(u_h^{\text{EG}}) \cdot \mathbf{n}_e) ds \\ + \sum_{e \in \mathcal{E}_i} \int_{K_e} \varphi_i \nabla \cdot \mathbf{f}(u_h^{\text{EG}}) d\mathbf{x} = 0, \quad i = 1, \dots, N_h \end{aligned} \quad (20)$$

for the nodal values of the CG component u_h . The union $\bar{\Omega}_i = \cup_{e \in \mathcal{E}_i} K_e$ of elements that contain the vertex \mathbf{x}_i represents the compact support of the basis function φ_i .

To derive a high-order semi-discrete scheme that is better suited for limiting, we first modify the last term on the left-hand side of (20) using the linear Taylor approximation (cf. [28])

$$\mathbf{f}(u_h^{\text{EG}}) = \mathbf{f}(u_h + \delta u_h) \approx \mathbf{f}(u_h) + \mathbf{f}'(u_h) \delta u_h. \quad (21)$$

Next, we replace $\mathbf{f}(u_h)$ by the *group finite element* (GFE) interpolant [11, 36, 37]

$$\mathbf{f}_h(u_h) = \sum_{j=1}^{N_h} \mathbf{f}(u_j) \varphi_j. \quad (22)$$

This modification corresponds to using inexact nodal quadrature for volume integrals. For

$$\int_{\partial K_e \cap \partial \Omega} \varphi_i (\mathcal{F}(u_{h,e}^-, u_{h,e}^+; \mathbf{n}_e) - \mathbf{f}(u_h^{\text{EG}}) \cdot \mathbf{n}_e) ds,$$

we use the ‘lumped’ GFE approximation (cf. [23, Eq. (3.118)])

$$\sum_{e' \in \mathcal{E}'_e} \sigma_{i,ee'} [\mathcal{F}(u_i, \hat{u}_{i,ee'}; \mathbf{n}_{ee'}) - \mathbf{f}(u_i) \cdot \mathbf{n}_{ee'}],$$

where $\mathcal{E}'_e = \{e' \in \mathcal{Z}_e : e' > E_h\}$ is the set of second subscripts of $S_{ee'} \subset \partial K_e \cap \partial\Omega$ and

$$\sigma_{i,ee'} = \int_{S_{ee'}} \varphi_i ds, \quad \hat{u}_{i,ee'} = \frac{1}{\sigma_{i,ee'}} \int_{S_{ee'}} \varphi_i u_{h,e}^+ ds.$$

Finally, we modify the time derivative term by using the convenient approximation

$$\int_{K_e} \varphi_i \frac{\partial u_h^{\text{EG}}}{\partial t} d\mathbf{x} \approx \left(\int_{K_e} \varphi_i d\mathbf{x} \right) \frac{du_i}{dt} + \int_{K_e} \varphi_i (\dot{u}_h - \dot{u}_i) d\mathbf{x},$$

where u_i is the time-dependent value of the CG component u_h at the vertex \mathbf{x}_i . Following Kuzmin et al. [33], we reconstruct the nodal values of $\dot{u}_h = \sum_{j=1}^{N_h} \dot{u}_j \varphi_j$ as follows:

$$\dot{u}_i = \frac{1}{|\Omega_i|} \sum_{e \in \mathcal{E}_i} |K_e| \frac{dU_e}{dt} = \frac{1}{|\Omega_i|} \sum_{e \in \mathcal{E}_i} q_e^H, \quad |\Omega_i| = \sum_{e \in \mathcal{E}_i} |K_e|. \quad (23)$$

The resulting system of evolution equations for the CG nodal values reads

$$\begin{aligned} \left(\sum_{e \in \mathcal{E}} \int_{K_e} \varphi_i d\mathbf{x} \right) \frac{du_i}{dt} &= \sum_{e \in \mathcal{E}} \int_{K_e} \varphi_i (\dot{u}_i - \dot{u}_h) d\mathbf{x} - \sum_{e \in \mathcal{E}} \sum_{e' \in \mathcal{E}'_e} \sigma_{i,ee'} [\mathcal{F}(u_i, \hat{u}_{i,ee'}; \mathbf{n}_{ee'}) - \mathbf{f}(u_i) \cdot \mathbf{n}_{ee'}] \\ &\quad - \sum_{e \in \mathcal{E}_i} \sum_{j \in N^e} \left(\int_{K_e} \varphi_i \nabla \varphi_j d\mathbf{x} \right) \cdot \mathbf{f}(u_j) \\ &\quad + \sum_{e \in \mathcal{E}_i} \delta u_e \int_{K_e} \nabla \varphi_i \cdot \mathbf{f}'(u_h) d\mathbf{x}, \quad i = 1, \dots, N_h \end{aligned} \quad (24)$$

and represents a second-order perturbation of (20). While it is possible to correct the corresponding errors in the limiting step, doing so would make the algorithms to be presented in Section 5 more complicated without having any significant positive impact on the accuracy of numerical solutions. Therefore, we use (24) rather than (20) as the high-order target for limiting.

To write system (24) in a matrix form, we need to introduce some further notation. Let

$$\begin{aligned} m_{ij} &= \sum_{e \in \mathcal{E}_i \cap \mathcal{E}_j} m_{ij}^e, & m_{ij}^e &= \int_{K_e} \varphi_i \varphi_j d\mathbf{x}, \\ m_i &= \sum_{e \in \mathcal{E}_i} m_i^e, & m_i^e &= \sum_{j \in N^e} m_{ij}^e = \int_{K_e} \varphi_i d\mathbf{x}, \\ \mathbf{c}_{ij} &= \sum_{e \in \mathcal{E}_i \cap \mathcal{E}_j} \mathbf{c}_{ij}^e, & \mathbf{c}_{ij}^e &= \int_{K_e} \varphi_i \nabla \varphi_j d\mathbf{x} \end{aligned}$$

denote the coefficients of the consistent mass matrix $M_C = (m_{ij})_{i,j=1}^{N_h}$, of its lumped counterpart $M_L = \text{diag}(m_i)_{i=1}^{N_h}$, and of the discrete gradient operator $\mathbf{C} = (\mathbf{c}_{ij})_{i,j=1}^{N_h}$. Note that

$$\mathbf{c}_{ji} = -\mathbf{c}_{ij} + \sum_{e \in \mathcal{E}_i} \int_{\partial K_e \cap \partial\Omega} \varphi_i \varphi_j \mathbf{n} ds, \quad \mathbf{c}_{ji}^e = -\mathbf{c}_{ij}^e + \int_{\partial K_e} \varphi_i \varphi_j \mathbf{n} ds.$$

Adopting the above notation, we write the evolution equations (24) in the equivalent form

$$m_i \frac{du_i}{dt} = \sum_{e \in \mathcal{E}_i} \sum_{j \in \mathcal{N}^e} m_{ij}^e (\dot{u}_i - \dot{u}_j) - \sum_{e \in \mathcal{E}_i} \sum_{e' \in \mathcal{E}_e} \sigma_{i,ee'} [\mathcal{F}(u_i, \hat{u}_{i,ee'}; \mathbf{n}_{ee'}) - \mathbf{f}(u_i) \cdot \mathbf{n}_{ee'}] \\ - \sum_{e \in \mathcal{E}_i} \sum_{j \in \mathcal{N}^e} \mathbf{c}_{ij}^e \cdot \mathbf{f}(u_j) + \sum_{e \in \mathcal{E}_i} (U_e - \bar{u}_e) \int_{K_e} \nabla \varphi_i \cdot \mathbf{f}'(u_h) d\mathbf{x} =: \mathbf{g}_i^H, \quad i = 1, \dots, N_h. \quad (25)$$

The matrix form of this high-order semi-discrete problem for CG nodal values is given by

$$M_L \frac{d\mathbf{u}}{dt} = \mathbf{g}^H(\mathbf{U}, \mathbf{u}), \quad (26)$$

where $\mathbf{g}^H = (g_i^H)_{i=1}^{N_h}$ is the global vector containing the right-hand sides of system (25).

4. Algebraic splitting

In Section 3, we have shown that the cell averages U_e and CG nodal values u_i of a high-order EG approximation u_h^{EG} to the solution of problem (1) satisfy the nonlinear system

$$\begin{bmatrix} \bar{M} & 0 \\ 0 & M_L \end{bmatrix} \frac{d}{dt} \begin{bmatrix} \mathbf{U} \\ \mathbf{u} \end{bmatrix} = \begin{bmatrix} \mathbf{q}^H(\mathbf{U}, \mathbf{u}) \\ \mathbf{g}^H(\mathbf{U}, \mathbf{u}) \end{bmatrix} \quad (27)$$

of coupled semi-discrete subproblems (19) and (26) for $\mathbf{U} = (U_e)_{e=1}^{E_h}$ and $\mathbf{u} = (u_i)_{i=1}^{N_h}$. The DG components $\delta u_e = U_e - \bar{u}_e$ are uniquely determined by the cell averages of u_h^{EG} and u_h .

To prepare the ground for the derivation of limiting techniques in Section 5, we need to split the high-order system (27) into a property-preserving low-order part and an antidiffusive correction term. The general form of such an algebraic splitting is given by [33]

$$\begin{bmatrix} \bar{M} & 0 \\ 0 & M_L \end{bmatrix} \frac{d}{dt} \begin{bmatrix} \mathbf{U} \\ \mathbf{u} \end{bmatrix} = \begin{bmatrix} \mathbf{q}^L(\mathbf{U}) + \bar{\mathbf{f}}(\mathbf{U}, \mathbf{u}) \\ \mathbf{g}^L(\mathbf{u}) + \mathbf{f}(\mathbf{U}, \mathbf{u}) \end{bmatrix}. \quad (28)$$

The components of the vectors $\bar{\mathbf{f}} = (\bar{f}_e)_{e=1}^{E_h}$ and $\mathbf{f} = (f_i)_{i=1}^{N_h}$ should admit decompositions

$$\bar{f}_e = \sum_{e' \in \mathcal{Z}_e} F_{ee'}, \quad f_i = \sum_{e \in \mathcal{E}_i} f_i^e$$

into numerical fluxes $F_{ee'}$ and element contributions f_i^e such that

$$F_{ee'} + F_{e'e} = 0, \quad \sum_{i \in \mathcal{N}^e} f_i^e = 0. \quad (29)$$

These zero sum properties must be preserved by limiters to guarantee discrete conservation.

The right-hand sides $\mathbf{q}^L = (q_e^L)_{e=1}^{E_h}$ and $\mathbf{g}^L = (g_i^L)_{i=1}^{N_h}$ of the low-order (LO) semi-discrete problems for \mathbf{U} and \mathbf{u} must ensure the validity of all relevant constraints for a solution of

$$\begin{bmatrix} \bar{M} & 0 \\ 0 & M_L \end{bmatrix} \frac{d}{dt} \begin{bmatrix} \mathbf{U} \\ \mathbf{u} \end{bmatrix} = \begin{bmatrix} \mathbf{q}^L(\mathbf{U}) \\ \mathbf{g}^L(\mathbf{u}) \end{bmatrix}. \quad (30)$$

In the remainder of this section, we present a splitting that provides the above properties.

4.1. Low-order semi-discrete problem for EG cell averages

A natural choice of the low-order scheme for \mathbf{U} is the finite volume LLF method [23, 34]

$$|K_e| \frac{dU_e}{dt} = - \sum_{e' \in \mathcal{Z}_e} \int_{S_{ee'}} \mathcal{F}(U_e^-, U_e^+; \mathbf{n}_{ee'}) ds =: q_e^L, \quad e = 1, \dots, E_h, \quad (31)$$

in which the LLF fluxes depend on the internal state $U_e^- = U_e$ and the external state

$$U_e^+ = \begin{cases} u_{\text{in}} & \text{on } \Gamma^{\text{in}} \\ U_e & \text{on } \Gamma^{\text{out}} \\ U_{e'} & \text{on } S_{ee'} = \partial K_e \cap \partial K_{e'}, \quad e' \leq E_h. \end{cases}$$

This approximation is known to be bound-preserving and entropy stable [23, 34]. Therefore, it is widely used as the LO component of modal DG methods equipped with flux and/or slope limiters. The matrix form of the corresponding semi-discrete problem reads

$$\bar{M} \frac{d\mathbf{U}}{dt} = \mathbf{q}^L(\mathbf{U}). \quad (32)$$

In contrast to $\mathbf{q}^H(\mathbf{U}, \mathbf{u})$, the right-hand side of (32) is independent of \mathbf{u} . Therefore, the LO cell averages evolve independently from the LO nodal values of the CG component u_h .

The difference between the right-hand sides of equations (17) and (31) is given by

$$\begin{aligned} \bar{f}_e &= q_e^H - q_e^L = \sum_{e' \in \mathcal{Z}_e} \int_{S_{ee'}} [\mathcal{F}(U_e^-, U_e^+; \mathbf{n}_{ee'}) - \mathcal{F}(u_{h,e}^-, u_{h,e}^+; \mathbf{n}_e)] ds \\ &= \sum_{e' \in \mathcal{Z}_e} |S_{ee'}| (H_{ee'}^{\mathbb{Q}_0} - H_{ee'}^{\mathbb{Q}_1}) = \sum_{e' \in \mathcal{Z}_e} F_{ee'}, \end{aligned}$$

where $H_{ee'}^{\mathbb{Q}_0}$ is the low-order counterpart of the LLF flux $H_{ee'}^{\mathbb{Q}_1}$ defined by (18) and

$$F_{ee'} = |S_{ee'}| (H_{ee'}^{\mathbb{Q}_0} - H_{ee'}^{\mathbb{Q}_1}) = -F_{e'e} \quad (33)$$

are the raw antidiffusive fluxes that constitute the component \bar{f}_e of the vector $\bar{\mathbf{f}}(\mathbf{U}, \mathbf{u})$ in (28).

4.1.1. Low-order semi-discrete problem for CG nodal values

An algebraic CG version of the LLF method (31) approximates the HO scheme (25) by [38]

$$\begin{aligned} m_i \frac{du_i}{dt} &= - \sum_{e \in \mathcal{E}_i} \sum_{e' \in \mathcal{E}'_e} \sigma_{i,ee'} [\mathcal{F}(u_i, \hat{u}_{i,ee'}; \mathbf{n}_{ee'}) - \mathbf{f}(u_i) \cdot \mathbf{n}_{ee'}] \\ &+ \sum_{e \in \mathcal{E}_i} \sum_{j \in \mathcal{N}^e} [d_{ij}^e u_j - \mathbf{c}_{ij}^e \cdot \mathbf{f}(u_j)] =: g_i^L, \quad i = 1, \dots, N_h. \end{aligned} \quad (34)$$

The LLF graph viscosity coefficients

$$d_{ij}^e = \begin{cases} \max(\lambda_{ij}^e |\mathbf{c}_{ij}^e|, \lambda_{ji}^e |\mathbf{c}_{ji}^e|) & \text{if } j \in \mathcal{N}^e, j \neq i, \\ - \sum_{k \in \mathcal{N}^e \setminus \{i\}} d_{ik}^e & \text{if } j \in \mathcal{N}^e, j = i, \\ 0 & \text{otherwise} \end{cases} \quad (35)$$

depend on $\lambda_{ij}^e = \lambda_{\max}(u_i, u_j; \mathbf{n}_{ij})$, where $\mathbf{n}_{ij} = \frac{\mathbf{e}_{ij}}{|\mathbf{e}_{ij}^e|}$ and $\lambda_{\max}(u_L, u_R; \mathbf{n})$ is defined as in (11). The matrix form of the semi-discrete scheme (34) is given by

$$M_L \frac{d\mathbf{u}}{dt} = \mathbf{g}^L(\mathbf{u}). \quad (36)$$

Since the right-hand side $\mathbf{g}^L(\mathbf{u})$ is independent of \mathbf{U} , so is a solution \mathbf{u} of this LO system.

A comparison of the spatial semi-discretizations (25) and (34) reveals that

$$\begin{aligned} f_i &= g_i^H - g_i^L = \sum_{e \in \mathcal{E}_i} \sum_{j \in \mathcal{N}^e} [m_{ij}^e (\dot{u}_i - \dot{u}_j) + d_{ij}^e (u_i - u_j)] \\ &\quad + \sum_{e \in \mathcal{E}_i} (U_e - \bar{u}_e) \int_{K_e} \nabla \varphi_i \cdot \mathbf{f}'(u_h) d\mathbf{x} = \sum_{e \in \mathcal{E}_i} f_i^e. \end{aligned}$$

The individual element contributions f_i^e to this component of $\mathbf{f}(\mathbf{U}, \mathbf{u})$ are defined by

$$f_i^e = \sum_{j \in \mathcal{N}^e} [m_{ij}^e (\dot{u}_i - \dot{u}_j) + d_{ij}^e (u_i - u_j)] + (U_e - \bar{u}_e) \int_{K_e} \nabla \varphi_i \cdot \mathbf{f}'(u_h) d\mathbf{x}. \quad (37)$$

To prove the zero sum property required in (29), we first notice that $m_{ij}^e = m_{ji}^e$ and $d_{ij}^e = d_{ji}^e$ by definition. The Lagrange basis functions φ_i of the CG- \mathbb{Q}_1 space V_h form a partition of unity, i.e., $\sum_{i \in \mathcal{N}^e} \varphi_i \equiv 1$. It follows that $\sum_{i \in \mathcal{N}^e} \nabla \varphi_i \equiv \mathbf{0}$ and $\sum_{i \in \mathcal{N}^e} f_i^e = 0$, as desired.

5. Property-preserving limiters

Given the algebraic splitting (28) of the high-order spatial semi-discretization (27), we can proceed to constructing a property-preserving EG approximation of the form

$$\begin{bmatrix} \bar{M} & 0 \\ 0 & M_L \end{bmatrix} \frac{d}{dt} \begin{bmatrix} \mathbf{U} \\ \mathbf{u} \end{bmatrix} = \begin{bmatrix} \mathbf{q}^L(\mathbf{U}) + \bar{\mathbf{f}}^*(\mathbf{U}, \mathbf{u}) \\ \mathbf{g}^L(\mathbf{u}) + \mathbf{f}^*(\mathbf{U}, \mathbf{u}) \end{bmatrix}, \quad (38)$$

where the vectors $\bar{\mathbf{f}}^* = (\bar{f}_e^*)_{e=1}^{E_h}$ and $\mathbf{f}^* = (f_i^*)_{i=1}^{N_h}$ are composed from

$$\bar{f}_e^* = \sum_{e' \in \mathcal{Z}_e} F_{ee'}^*, \quad f_i^* = \sum_{e \in \mathcal{E}_i} f_i^{e,*}.$$

The constrained approximations $F_{ee'}^* \approx F_{ee'}$ and $f_i^{e,*} \approx f_i^e$ should satisfy the zero sum conditions

$$F_{ee'}^* + F_{e'e}^* = 0, \quad \sum_{i \in \mathcal{N}^e} f_i^{e,*} = 0. \quad (39)$$

Additionally, the limiters to be presented below will ensure the validity of local discrete maximum principles (DMPs) and entropy stability of the semi-discrete schemes for \mathbf{U} and \mathbf{u} .

5.1. Limiting criteria

A closed interval $\mathcal{G} = [u^{\min}, u^{\max}]$ represents an invariant domain of the scalar hyperbolic problem (1) if preservation of the global bounds u^{\min} and u^{\max} can be shown for exact solutions. We call the spatial semi-discretization (38) invariant domain preserving (IDP) if it produces admissible states $U_e(t) \in \mathcal{G}$ and $u_i(t) \in \mathcal{G}$ at any time $t > 0$. We need (38) to be IDP and, moreover, local extremum diminishing (LED) in the sense that the time derivatives of $U_e(t)$ and $u_i(t)$ are nonpositive/nonnegative at a local maximum/minimum [39, 40, 10, 23].

Suppose that there exist bounded solution-dependent coefficients $A_e \geq 0$ and $a_i \geq 0$ such that

$$\frac{dU_e}{dt} = \frac{q_e^L + \tilde{f}_e^*}{|K_e|} = A_e(\bar{U}_e^* - U_e), \quad e = 1, \dots, E_h, \quad (40)$$

$$\frac{du_i}{dt} = \frac{g_i^L + f_i^*}{m_i} = a_i(\bar{u}_i^* - u_i), \quad i = 1, \dots, N_h, \quad (41)$$

where $\bar{U}_e^* \in [U_e^{\min}, U_e^{\max}] \subseteq \mathcal{G}$ and $\bar{u}_i^* \in [u_i^{\min}, u_i^{\max}] \subseteq \mathcal{G}$ are some locally bound-preserving intermediate states. Then the semi-discrete scheme (38) is LED and its IDP property can be shown using Theorem 1 from [41]. For fully discrete schemes, preservation of local bounds by forward Euler stages is guaranteed if the time step Δt satisfies the CFL conditions [23, 41]

$$\Delta t A_e \leq 1, \quad e = 1, \dots, E_h, \quad (42)$$

$$\Delta t a_i \leq 1, \quad i = 1, \dots, N_h. \quad (43)$$

Let us now formulate additional constraints that imply the validity of semi-discrete entropy inequalities for a particular entropy pair $\{\eta(u), \mathbf{q}(u)\}$. According to Tadmor's theory [22], a cell entropy inequality for U_e holds under the sufficient condition (cf. [42, 20, 23])

$$(v(U_e) - v(U_{e'})) F_{ee'}^* \leq |S_{ee'}| \left((\boldsymbol{\psi}(U_{e'}) - \boldsymbol{\psi}(U_e)) \cdot \mathbf{n}_{ee'} + (v(U_e) - v(U_{e'})) H_{ee'}^{\mathbb{Q}_0} \right), \quad (44)$$

where $H_{ee'}^{\mathbb{Q}_0} = \mathcal{F}(U_e^-, U_e^+; \mathbf{n}_{ee'})$ is the low-order LLF flux, $v(u) = \eta'(u)$ is the entropy variable and $\boldsymbol{\psi}(u) = v(u)\mathbf{f}(u) - \mathbf{q}(u)$ is the entropy potential. In essence, Tadmor's condition (44) imposes an upper bound on the rate $(v(U_e) - v(U_{e'}))F_{ee'}^*$ of entropy production by the flux $F_{ee'}^*$.

The rate of entropy production by the element contribution $f_i^{e,*}$ is given by $(v(u_i) - \bar{v}_e)f_i^{e,*}$, where $\bar{v}_e = \frac{1}{|N^e|} \sum_{j \in N^e} v(u_j)$ is the arithmetic mean of $|N^e|$ nodal entropy variables. Adapting Tadmor's theory to the CG setting as in [20, 38], we impose the constraint

$$(v(u_i) - \bar{v}_e)f_i^{e,*} \leq \sum_{j \in N^e \setminus \{i\}} |\mathbf{c}_{ij}^e| \left((\boldsymbol{\psi}(u_j) - \boldsymbol{\psi}(u_i)) \cdot \mathbf{n}_{ij}^e + (v(u_i) - v(u_j))H_{ij}^{e,L} \right), \quad (45)$$

where

$$H_{ij}^{e,L} = \frac{\mathbf{f}(u_j) + \mathbf{f}(u_i)}{2} \cdot \mathbf{n}_{ij}^e - \frac{d_{ij}^e}{2|\mathbf{c}_{ij}^e|} (u_j - u_i), \quad \mathbf{n}_{ij}^e = \frac{\mathbf{c}_{ij}^e}{|\mathbf{c}_{ij}^e|}.$$

Note that $\sum_{i \in N_e} (v(u_i) - \bar{v}_e)f_i^{e,*} = \sum_{i \in N_e} v(u_i)f_i^{e,*}$ because $\sum_{i \in N_e} f_i^{e,*} = 0$ by (39). As shown in [38], this zero sum property of the element vector $(f_i^{e,*})_{i \in N^e}$ also implies the existence of numerical fluxes $f_{ij}^{e,*} = -f_{ji}^{e,*}$ such that $f_i^{e,*} = \sum_{j \in N^e \setminus \{i\}} f_{ij}^{e,*}$. It follows that

$$\sum_{i \in N_e} (v(u_i) - \bar{v}_e)f_i^{e,*} = \sum_{i \in N_e} v(u_i) \sum_{j \in N^e \setminus \{i\}} f_{ij}^{e,*} = \sum_{i \in N_e} \sum_{j \in N^e \setminus \{i\}} \frac{v(u_i) - v(u_j)}{2} f_{ij}^{e,*}.$$

Using this auxiliary result, the entropy stability property of the semi-discrete scheme for CG nodal values can be established as in [38, Thm. 3]. In practice, there is no need to calculate the fluxes $f_{ij}^{e,*}$ because the stability condition (45) is imposed directly on the sum $f_i^{e,*}$.

It remains to select or devise practical algorithms for enforcing the above constraints. In the next two subsections, we present the old and new limiters that we use for this purpose.

5.2. Monolithic limiting for EG cell averages

The flux limiting framework developed in [34, 42] for DG methods and in [33] for an EG discretization of the linear advection equation is directly applicable to our nonlinear problem for cell averages. By definition (10) of the LLF flux, the equation for U_e can be written as

$$\begin{aligned} |K_e| \frac{dU_e}{dt} &= - \sum_{e' \in \mathcal{Z}_e} |S_{ee'}| \left(\frac{\mathbf{f}(U_e) + \mathbf{f}(U_{e'})}{2} \cdot \mathbf{n}_{ee'} - \frac{\lambda_{ee'}}{2} (U_{e'} - U_e) \right) + \sum_{e' \in \mathcal{Z}_e} F_{ee'}^* \\ &= \sum_{e' \in \mathcal{Z}_e} (|S_{ee'}| \lambda_{ee'} (\bar{U}_{ee'} - U_e) + F_{ee'}^*) = \sum_{e' \in \mathcal{Z}_e} |S_{ee'}| \lambda_{ee'} (\bar{U}_{ee'}^* - U_e), \end{aligned} \quad (46)$$

where [19, 34, 41]

$$\bar{U}_{ee'} = \frac{U_{e'} + U_e}{2} - \frac{\mathbf{f}(U_{e'}) - \mathbf{f}(U_e)}{2\lambda_{ee'}} \cdot \mathbf{n}_{ee'}, \quad \bar{U}_{ee'}^* = \bar{U}_{ee'} + \frac{F_{ee'}^*}{|S_{ee'}| \lambda_{ee'}}.$$

The low-order *bar state* $\bar{U}_{ee'} = \bar{U}_{e'e}$ is a convex combination of $U_{e'}$ and U_e . This can be shown as in [19] using the mean value theorem and the definition of $\lambda_{ee'}$ as a local upper bound for the wave speed $|\mathbf{f}'(u) \cdot \mathbf{n}_{ee'}|$. It follows that $\bar{U}_{ee'} \in \mathcal{G} = [u^{\min}, u^{\max}]$ whenever $U_e, U_{e'} \in \mathcal{G}$. For any choice of local bounds $U_e^{\min} \in [u^{\min}, \bar{U}_{ee'}]$ and $U_e^{\max} \in [\bar{U}_{ee'}, u^{\max}]$, the inequality constraints

$$U_e^{\min} \leq \bar{U}_{ee'} + \frac{F_{ee'}^*}{\lambda_{ee'}} \leq U_e^{\max}, \quad U_{e'}^{\min} \leq \bar{U}_{ee'} - \frac{F_{ee'}^*}{\lambda_{ee'}} \leq U_{e'}^{\max}, \quad (47)$$

can always be enforced by limiting the magnitude of the flux $F_{ee'}^* = -F_{e'e}^*$. The validity of (47) implies that $\bar{U}_{ee'}^* \in [U_e^{\min}, U_e^{\max}]$ and $\bar{U}_{e'e}^* \in [U_{e'}^{\min}, U_{e'}^{\max}]$. The IDP and LED properties follow from the fact that (46) can be written in the form (40) with [41]

$$A_e = \frac{1}{|K_e|} \sum_{e' \in \mathcal{Z}_e} |S_{ee'}| \lambda_{ee'}, \quad \bar{U}_e^* = \frac{1}{A_e |K_e|} \sum_{e' \in \mathcal{Z}_e} |S_{ee'}| \lambda_{ee'} \bar{U}_{ee'}^*,$$

where \bar{U}_e^* is a convex combination of the bound-preserving intermediate states $\bar{U}_{ee'}^*$.

Following Kuzmin et al. [33], we define the local bounds for EG cell averages as follows:

$$\begin{aligned} U_e^{\max} &:= \max \left\{ \max_{\partial K_e \cap \Gamma^{\text{in}}} u_{\text{in}}, \max_{i \in \mathcal{N}^e} \left\{ \max_{e' \in \mathcal{E}_i} U_{e'}, u_i \right\} \right\}, \\ U_e^{\min} &:= \min \left\{ \min_{\partial K_e \cap \Gamma^{\text{in}}} u_{\text{in}}, \min_{i \in \mathcal{N}^e} \left\{ \min_{e' \in \mathcal{E}_i} U_{e'}, u_i \right\} \right\} \end{aligned}$$

and calculate bound-preserving (BP) approximations $F_{ee'}^{\text{BP}} = -F_{e'e}^{\text{BP}}$ to the target fluxes $F_{ee'} = -F_{e'e}$ defined by (33) using the finite volume / DG version

$$F_{ee'}^{\text{BP}} = \begin{cases} \min \left\{ F_{ee'}, |S_{ee'}| \lambda_{ee'} \min \left\{ U_e^{\max} - \bar{U}_{ee'}, \bar{U}_{e'e} - U_{e'}^{\min} \right\} \right\} & \text{if } F_{ee'} > 0, \\ \max \left\{ F_{ee'}, |S_{ee'}| \lambda_{ee'} \max \left\{ U_e^{\min} - \bar{U}_{ee'}, \bar{U}_{e'e} - U_{e'}^{\max} \right\} \right\} & \text{if } F_{ee'} \leq 0 \end{cases}$$

of the monolithic convex limiting formula derived in [19] in the context of CG discretizations.

To enforce Tadmor's condition (44) using a limiter-based entropy fix (cf. [42, 38, 20]), we constrain the final flux $F_{ee'}^* = \alpha_{ee'} F_{ee'}^{\text{BP}}$ of the MCL scheme (46) using the correction factor

$$\alpha_{ee'} = \begin{cases} \frac{Q_{ee'}}{P_{ee'}} & \text{if } P_{ee'} > Q_{ee'}, \\ 1 & \text{otherwise,} \end{cases}$$

where

$$P_{ee'} = (v(U_{e'}) - v(U_e)) F_{ee'}^{\text{BP}}, \quad Q_{ee'} = Q_{ee'}^+ + \min\{0, Q_{ee'}^-\} \geq 0.$$

The components $Q_{ee'}^\pm$ of the entropy-dissipative bound $Q_{ee'}$ are defined by (cf. [42])

$$\begin{aligned} Q_{ee'}^+ &= |S_{ee'}| (v(U_{e'}) - v(U_e)) \frac{\lambda_{ee'}}{2} (U_{e'} - U_e), \\ Q_{ee'}^- &= |S_{ee'}| \left(\psi(U_{e'}) - \psi(U_e) - (v(U_{e'}) - v(U_e)) \frac{\mathbf{f}(U_{e'}) + \mathbf{f}(U_e)}{2} \right) \cdot \mathbf{n}_{ee'}. \end{aligned}$$

The nonnegativity of $Q_{ee'}$ follows from the fact that the low-order LLF scheme is entropy stable (see, e.g., [23]). It is easy to verify that $Q_{ee'}$ is bounded above by the right-hand side of (44) and that $(v(U_{e'}) - v(U_e)) F_{ee'}^* \leq Q_{ee'}$ for our choice of the correction factor $\alpha_{ee'} = \alpha_{e'e}$.

Since the above limiting strategy for $F_{ee'}^*$ is not new, we refer the reader to the original publications [34, 33, 42] and to the book [23] for detailed explanations and proofs.

5.3. Monolithic limiting for CG nodal values

The limiter that we apply to the element contributions $f_i^{e,*}$ is an entropy-stable extension of the element-based MCL algorithms proposed in [33],[23, Sec. 6.3]. We first express the flux-corrected equation for the CG nodal value u_i in terms of intermediate states as follows:

$$\begin{aligned} m_i \frac{du_i}{dt} &= - \sum_{e \in \mathcal{E}_i} \sum_{e' \in \mathcal{E}'_e} \sigma_{i,ee'} [\mathcal{F}(u_i, \hat{u}_{i,ee'}; \mathbf{n}_{ee'}) - \mathbf{f}(u_i) \cdot \mathbf{n}_{ee'}] \\ &\quad + \sum_{e \in \mathcal{E}_i} \sum_{j \in \mathcal{N}^e} [d_{ij}^e u_j - \mathbf{c}_{ij}^e \cdot \mathbf{f}(u_j)] + \sum_{e \in \mathcal{E}_i} f_i^{e,*} \\ &= \sum_{e \in \mathcal{E}_i} \sum_{e' \in \mathcal{E}'_e} \frac{\sigma_{i,ee'}}{2} [\lambda_{ee'} (\hat{u}_{i,ee'} - u_i) - (\mathbf{f}(\hat{u}_{i,ee'}) - \mathbf{f}(u_i)) \cdot \mathbf{n}_{ee'}] \\ &\quad + \sum_{e \in \mathcal{E}_i} \sum_{j \in \mathcal{N}^e \setminus \{i\}} [d_{ij}^e (u_j - u_i) - (\mathbf{f}(u_j) - \mathbf{f}(u_i)) \cdot \mathbf{c}_{ij}^e] + \sum_{e \in \mathcal{E}_i} f_i^{e,*} \\ &= \sum_{e \in \mathcal{E}_i} \left[\sum_{e' \in \mathcal{E}'_e} \sigma_{i,ee'} \lambda_{ee'} (\bar{u}_{i,ee'} - u_i) + \sum_{j \in \mathcal{N}^e \setminus \{i\}} 2d_{ij}^e (\bar{u}_{ij}^e - u_i) + f_i^{e,*} \right] \\ &= \sum_{e \in \mathcal{E}_i} [\gamma_i^e (\bar{u}_i^e - u_i) + f_i^{e,*}] = \sum_{e \in \mathcal{E}_i} \gamma_i^e (\bar{u}_i^{e,*} - u_i), \end{aligned} \tag{48}$$

where

$$\begin{aligned}\bar{u}_{i,ee'} &= \frac{\hat{u}_{i,ee'} + u_i}{2} - \frac{(\mathbf{f}(\hat{u}_{i,ee'}) - \mathbf{f}(u_i)) \cdot \mathbf{n}_{ee'}}{2\lambda_{ee'}}, & \bar{u}_{ij}^e &= \frac{u_j + u_i}{2} - \frac{(\mathbf{f}(u_j) - \mathbf{f}(u_i)) \cdot \mathbf{c}_{ij}^e}{2d_{ij}^e}, \\ \bar{u}_i^e &= \frac{1}{\gamma_i^e} \left[\sum_{e' \in \mathcal{E}'_e} \sigma_{i,ee'} \lambda_{ee'} \bar{u}_{i,ee'} + \sum_{j \in \mathcal{N}^e \setminus \{i\}} 2d_{ij}^e \bar{u}_{ij}^e \right], & \bar{u}_i^{e,*} &= \bar{u}_i^e + \frac{f_i^{e,*}}{\gamma_i^e}, \\ \gamma_i^e &= \sum_{e' \in \mathcal{E}'_e} \sigma_{i,ee'} \lambda_{ee'} + \sum_{j \in \mathcal{N}^e \setminus \{i\}} 2d_{ij}^e.\end{aligned}$$

Therefore, equation (48) can be written in the form (41) with

$$a_i = \frac{1}{m_i} \sum_{e \in \mathcal{E}_i} \gamma_i^e, \quad \bar{u}_i^* = \frac{1}{a_i m_i} \sum_{e \in \mathcal{E}_i} \gamma_i^e \bar{u}_i^{e,*}.$$

To ensure that the intermediate state $\bar{u}_i^{e,*}$ is bounded by

$$u_i^{\max} = \max \left\{ u_i, \max_{e \in \mathcal{E}_i} \bar{u}_i^e \right\} \quad \text{and} \quad u_i^{\min} = \min \left\{ u_i, \min_{e \in \mathcal{E}_i} \bar{u}_i^e \right\},$$

we impose the MCL constraints

$$u_i^{\min} \leq \bar{u}_i^e + \frac{f_i^{e,*}}{\gamma_i^e} \leq u_i^{\max}. \quad (49)$$

To satisfy the entropy stability condition (45), we additionally require that

$$(v(u_i) - \bar{v}_e) f_i^{e,*} \leq \sum_{j \in \mathcal{N}^e \setminus \{i\}} [Q_{ij}^{e,+} + \min\{0, Q_{ij}^{e,-}\}] =: Q_i^e, \quad (50)$$

where Q_i^e is a nonnegative production bound depending on

$$\begin{aligned}Q_{ij}^{e,+} &= (v(u_j) - v(u_i)) \frac{d_{ij}^e}{2} (u_j - u_i), \\ Q_{ij}^{e,-} &= \left(\psi(u_j) - \psi(u_i) - (v(u_j) - v(u_i)) \frac{\mathbf{f}(u_j) + \mathbf{f}(u_i)}{2} \right) \cdot \mathbf{c}_{ij}^e.\end{aligned}$$

For $f_i^{e,*} = \alpha_i^e f_i^e$ with $\alpha_i^e \in [0, 1]$, condition (50) is equivalent to

$$\alpha_i^e P_i^e \leq Q_i^e, \quad P_i^e := (v(u_i) - \bar{v}_e) f_i^e.$$

Adopting a clip-and-scale limiting strategy (cf. [17, 33, 23]), we first apply

$$\alpha_i^e = \begin{cases} \frac{Q_i^e}{P_i^e} & \text{if } P_i^e > Q_i^e, \\ 1 & \text{otherwise} \end{cases}$$

to f_i^e defined by (37). Then we calculate the clipped element contributions

$$\tilde{f}_i^{e,*} = \begin{cases} \min\{\alpha_i^e f_i^e, \gamma_i^e (u_i^{\max} - \bar{u}_i^e)\} & \text{if } f_i^e > 0, \\ \max\{\alpha_i^e f_i^e, \gamma_i^e (u_i^{\min} - \bar{u}_i^e)\} & \text{if } f_i^e \leq 0. \end{cases}$$

It is easy to verify that conditions (49) and (50) hold for $f_i^{e,*} = \tilde{f}_i^{e,*}$. However, this definition of $f_i^{e,*}$ does not generally ensure the validity of the zero sum condition $\tilde{f}_e^+ + \tilde{f}_e^- = 0$ for

$$\tilde{f}_e^+ = \sum_{i \in \mathcal{N}^e} \max\{0, f_i^{e,*}\}, \quad \tilde{f}_e^- = \sum_{i \in \mathcal{N}^e} \min\{0, f_i^{e,*}\}.$$

In the scaling stage of our entropic MCL procedure, we calculate (cf. [17, 33])

$$f_i^{e,*} = \begin{cases} \left(-\frac{\tilde{f}_e^-}{\tilde{f}_e^+}\right) \tilde{f}_i^{e,*} & \text{if } \tilde{f}_e^+ + \tilde{f}_e^- > 0 \text{ and } \tilde{f}_i^{e,*} > 0, \\ \left(-\frac{\tilde{f}_e^+}{\tilde{f}_e^-}\right) \tilde{f}_i^{e,*} & \text{if } \tilde{f}_e^+ + \tilde{f}_e^- < 0 \text{ and } \tilde{f}_i^{e,*} < 0, \\ \tilde{f}_i^{e,*} & \text{otherwise.} \end{cases} \quad (51)$$

This final result satisfies the zero sum condition $\sum_{i \in \mathcal{N}^e} f_i^{e,*} = 0$ in addition to (49) and (50).

Remark 3. By default, the monolithic limiting strategy for (38), as presented in Sections 5.2 and 5.3, enforces both preservation of local bounds and entropy stability. The inequality constraints associated with either of these properties can be modified or deactivated for testing purposes. For example, flux limiters based solely on conditions (47) and (49) would disregard the entropy stability conditions, as in [23, 33, 34]. Several comparisons between bound-preserving limiting strategies without and with optional entropy fixes are performed in Section 7.

5.4. Constrained projection of output data

The limiting techniques presented so far guarantee preservation of local bounds for the EG cell averages and CG nodal values. However, no discrete maximum principle generally holds for the restriction $u_h^{\text{EG}}|_{K_e} = u_h|_{K_e} + \delta u_e = u_h|_{K_e} + (U_e - \bar{u}_e)$ of the EG solution to a cell K_e . When it comes to visualizing the results or using them as input data in solvers for other equations, we project u_h^{EG} into the CG space V_h^{CG} using the flux-corrected remapping (FCR) algorithm presented in [33]. The nodal values of the standard L^2 projection $u_h^H = \sum_{j=1}^{N_h} u_j^H \varphi_j$ satisfy

$$\sum_{j \in \mathcal{N}_i} m_{ij} u_j^H = \sum_{e \in \mathcal{E}_i} \int_{K_e} u_h^{\text{EG}} \mathbf{d}\mathbf{x}, \quad i = 1, \dots, N_h.$$

The FCR scheme yields a bound-preserving approximation $u_h^{\text{FCR}} = \sum_{j=1}^{N_h} u_j^{\text{FCR}} \varphi_j$ such that

$$u_i^{\min, \text{FCR}} \leq u_i^{\text{FCR}} = u_i^L + \frac{1}{m_i} \sum_{e \in \mathcal{E}_i} \alpha_e^{\text{FCR}} f_i^{e, \text{FCR}} \leq u_i^{\max, \text{FCR}}, \quad i = 1, \dots, N_h, \quad (52)$$

where

$$u_i^{\max, \text{FCR}} = \max \left\{ \max_{e \in \mathcal{E}_i} U_e, \max_{j \in \mathcal{N}_i} u_j \right\}, \quad u_i^{\min, \text{FCR}} = \min \left\{ \min_{e \in \mathcal{E}_i} U_e, \min_{j \in \mathcal{N}_i} u_j \right\},$$

$$u_i^L = \frac{1}{m_i} \sum_{e \in \mathcal{E}_i} m_i^e U_e, \quad f_i^{e, \text{FCR}} = \int_{K_e} \varphi_i (u_i^H - u_h^H + u_h^{\text{EG}} - U_e) \mathbf{d}\mathbf{x},$$

$$\alpha_e^{\text{FCR}} = \min_{i \in N^e} \begin{cases} \min \left\{ 1, \frac{m_i^e(u_i^{\text{max,FCR}} - u_i^L)}{f_i^{e,\text{FCR}}} \right\} & \text{if } f_i^{e,\text{FCR}} > 0, \\ \min \left\{ 1, \frac{m_i^e(u_i^{\text{min,FCR}} - u_i^L)}{f_i^{e,\text{FCR}}} \right\} & \text{if } f_i^{e,\text{FCR}} < 0, \\ 1 & \text{otherwise.} \end{cases}$$

We plot u_h^{FCR} instead of u_h^{EG} in the figures that we present in Section 7. However, we do not overwrite u_h^{EG} by u_h^{FCR} and calculate the error norms using u_h^{EG} rather than u_h^{FCR} .

6. Temporal discretization

We discretize system (38) in time using Heun's method, a second-order explicit strong stability preserving Runge–Kutta method with two forward Euler updates (SSP-RK2). Let $\Delta t = T/N_T$ denote the constant time step corresponding to a uniform subdivision of the time interval $[0, T]$ into $N_T \in \mathbb{N}$ subintervals. Individual components of the global vectors

$$\mathbf{U}^n = (U_e^n)_{e=1}^{E_h} \quad \text{and} \quad \mathbf{u}^n = (u_i^n)_{i=1}^{N_h}$$

represent approximations to the EG cell averages and CG nodal values, respectively, at the time level $t^n = n\Delta t$, $0 \leq n \leq N_T$. Applying Heun's method to the coupled subproblems (40) and (41), we advance the degrees of freedom U_e^n and u_i^n to the time level t^{n+1} as follows:

1. First forward Euler step

$$\begin{aligned} U_e^{(n,1)} &= U_e^n + \Delta t A_e^n (\bar{U}_e^{n,*} - U_e^n), & e &= 1, \dots, E_h, \\ u_i^{(n,1)} &= u_i^n + \Delta t a_i^n (\bar{u}_i^{n,*} - u_i^n), & i &= 1, \dots, N_h. \end{aligned}$$

2. Second forward Euler step

$$\begin{aligned} U_e^{(n,2)} &= U_e^{(n,1)} + \Delta t A_e^{(n,1)} (\bar{U}_e^{(n,1),*} - U_e^{(n,1)}), & e &= 1, \dots, E_h, \\ u_i^{(n,2)} &= u_i^{(n,1)} + \Delta t a_i^{(n,1)} (\bar{u}_i^{(n,1),*} - u_i^{(n,1)}), & i &= 1, \dots, N_h. \end{aligned}$$

3. Final SSP-RK stage:

$$\begin{aligned} U_e^{n+1} &= \frac{1}{2} (U_e^{(2,n)} + U_e^n), & e &= 1, \dots, E_h, \\ u_i^{n+1} &= \frac{1}{2} (u_i^{(2,n)} + u_i^n), & i &= 1, \dots, N_h. \end{aligned}$$

If the CFL conditions (42) and (43) hold, each step produces a convex combination of old values. Therefore, discrete maximum principles are satisfied for the new ones. The DG components

$$\delta u_e^{n+1} = U_e^{n+1} - \bar{u}_e^{n+1}, \quad e = 1, \dots, E_h$$

are treated as derived quantities in our implementation of the EG method. The optional FCR postprocessing (see Section 5.4) ensures preservation of local bounds for projected output data.

7. Numerical results

In this section, we illustrate the capabilities of (individual components of) the proposed algorithm by running several numerical experiments. In particular, we perform grid convergence tests and apply the methods under investigation to two-dimensional benchmark problems. Throughout this section, the acronyms **HO** (High Order) and **LO** (Low Order) refer to the EG schemes defined in Sections 3 and 4, respectively. The one denoted by **BP-ES** enforces both preservation of local bounds and entropy stability, as described in Section 5. The method labeled **BP** differs from **BP-ES** in that the entropy fixes are deactivated to check if they are needed to ensure convergence towards correct weak solutions. In all numerical experiments, we use uniform rectangular meshes and codes implemented using the deal.II finite element library [43].

7.1. Example 1. Convergence test for a linear advection equation

First, we run the grid convergence test for the following linear advection equation

$$\frac{\partial u}{\partial t} + \nabla \cdot (\mathbf{v}u) = 0, \quad (53)$$

where $\mathbf{v} \equiv (1, 0)$ is the constant velocity. The computational domain is given by $\Omega = (0, 1)^2$. The inflow boundary condition is imposed on $\Gamma^{\text{in}} = \{(x, y) \in \partial\Omega : x = 0\}$, while the outflow boundary condition is applied otherwise. The exact solution is given by

$$u(x, y, t) = \cos(\pi(x - t)),$$

with the initial condition $u_0(x, y) = \cos(\pi x)$. We choose the square entropy $\eta(u) = u^2/2$ corresponding to the entropy flux $\mathbf{q}(u) = (u^2/2, 0)$. This setup extends a one-dimensional advection problem with the exact solution $u(x, t) = \cos(\pi(x - t))$ into the two-dimensional domain.

We test our LO, HO, BP and BP-ES schemes by running numerical simulations on seven uniformly refined meshes up to the final time $T = 0.5$. The mesh sizes range from $h = 2^{-2}$ to $h = 2^{-8}$. For numerical integration in time, we use the SSP-RK2 method (as presented in Section 6). To satisfy the CFL-like conditions (42) and (43), the time step $\Delta t = 0.025$ is also refined, maintaining a constant ratio of $\Delta t/h = 0.1$. We then use the global norms

$$\|u_h^{\text{EG}} - u\|_{l^\infty(L^1)} := \max_{0 \leq n \leq N} \|u_h^{\text{EG},n} - u^n\|_{L^1} \quad \text{and} \quad \|u_h^{\text{EG}} - u\|_{l^2(H^1)} := \sqrt{\sum_{n=1}^N \Delta t \|u_h^{\text{EG},n} - u^n\|_{H^1}^2}$$

to measure the numerical error $u_h^{\text{EG}} - u$. The convergence results are presented in Figure 3.

Figure 3a shows that our LO scheme achieves the expected first-order convergence rate in the $l^\infty(L^1)$ -norm. The BP-ES, BP and HO results exhibit nearly second-order convergence. In the final cycle, the convergence rate is 1.91 for both BP-ES and BP, while the HO error shrinks at the rate 1.98. These results align with those reported in [44, 45, 46]. The $l^2(H^1)$ errors are shown in Figure 3b. The LO convergence rate is 0.59 in the final cycle, while BP-ES, BP and HO achieve optimal first-order convergence rates 0.98, 0.99 and 1.02, respectively.

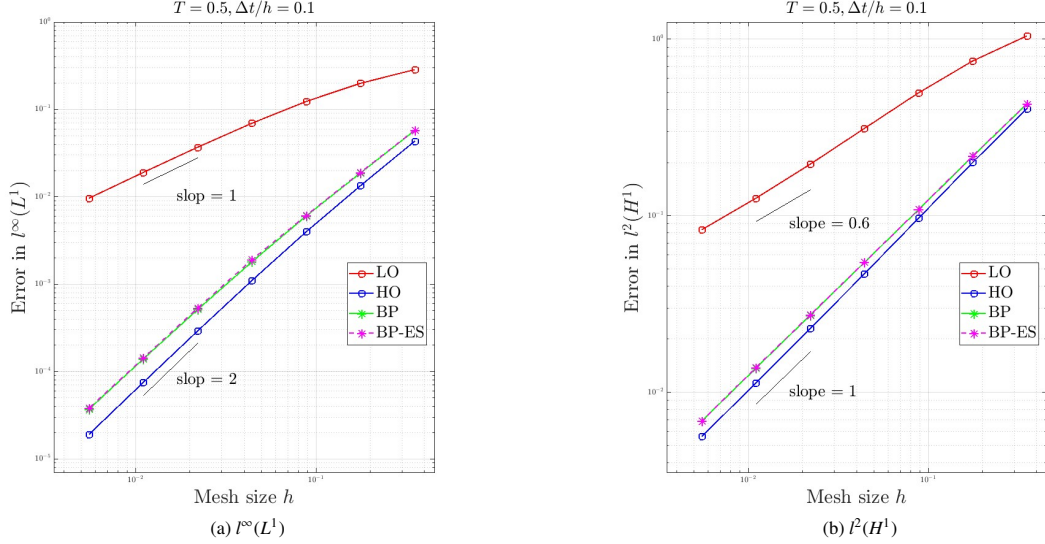


Figure 3: Example 1. The convergence behavior of EG errors for LO, HO, and BP schemes.

As expected, we obtain the optimal convergence rate for both BP and BP-ES with the employed limiters. Since the exact solution is smooth, the differences between the constrained EG approximations and the underlying HO scheme are insignificant.

7.2. Example 2. Convergence test for an inviscid Burgers equation

In this example, we examine the performance of our numerical schemes applied to the nonlinear inviscid Burgers equation

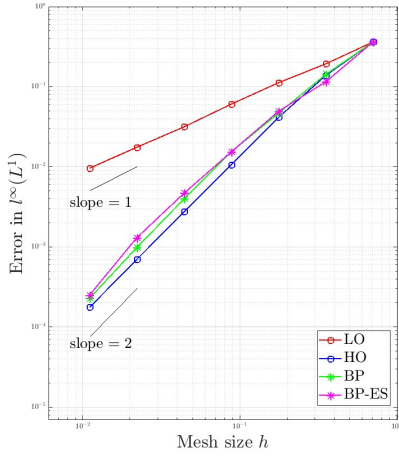
$$\frac{\partial u}{\partial t} + \nabla \cdot \left(\frac{u^2}{2} \mathbf{v} \right) = 0 \quad (55)$$

with $\mathbf{v} \equiv (1, 0)$ in the computational domain $\Omega = (0, 1)^2$. The inflow boundary condition is imposed on $\Gamma^{\text{in}} = \{(x, y) \in \partial\Omega : x = 0\}$, and the outflow boundary condition is applied elsewhere. The initial condition is given by $u_0(x, y) = \sin(2\pi x)$. For this nonlinear test, we choose the entropy $\eta(u) = u^4/4$ with the corresponding entropy flux $\mathbf{q}(u) = (u^5/5, 0)$.

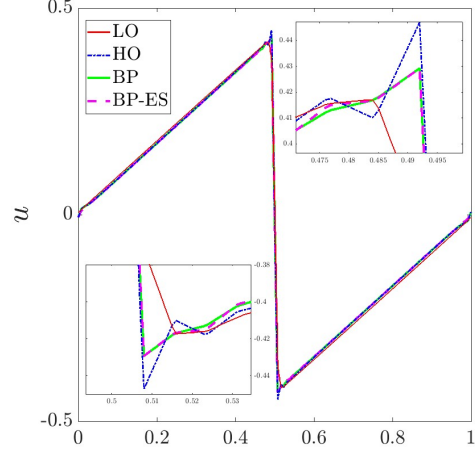
Note that the unique entropy solution develops a shock at the critical time $t_c = \frac{1}{2\pi}$. However, before t_c , the solution remains smooth and can be obtained using the method of characteristics [35]. To determine the exact solution value $u(\mathbf{x}, t) = u_0(\mathbf{x}_0)$ for $t < t_c$, we solve the nonlinear equation $\mathbf{x}_0 = \mathbf{x} - u_0(\mathbf{x}_0)\mathbf{v}t$ for \mathbf{x}_0 using fixed-point iterations. Similarly to Example 7.1, the problem that we consider in this nonlinear test is essentially one dimensional, although computations are performed in a two-dimensional domain.

We first test the convergence behavior of the LO, HO, BP, and BP-ES schemes by solving the Burgers equation (55) up to the final time $T = 0.1 < t_c$ on seven uniformly refined meshes ($h = 2^{-1}$ to $h = 2^{-7}$). The time step $\Delta t = 0.002h$ is also refined in each cycle.

The $l^\infty(L^1)$ -error of the EG solution u_h^{EG} is reported in Figure 4a. The unconstrained HO scheme exhibits second-order convergence at the rate 1.99 in the final cycle. This demonstrates that our baseline EG discretization of the nonlinear problem is second-order accurate, despite



(a) $T = 0.1$, $\Delta t/h = 0.002$



(b) $T = 1.0$, $h = 2^{-7}$, $\Delta t = 0.001$

Figure 4: Example 2. The diagrams show (a) error behavior and (b) solution profiles along the line $y = 0.5$.

the use of the linear Taylor approximation (21) and of the group finite element formulation (22). The convergence rate of the LO scheme is 0.87 in the final cycle, while the BP and BP-ES convergence rates become as high as 2.10 and 2.38, respectively. This indicates that the first-order error of the LO approximation is fully compensated in the limiting stage.

Next, we extend the final time to $T = 1.0 > t_c$ and run a BP-ES simulation of the propagating shock. In this test, we use the mesh with spacing $h = 2^{-7}$ and the time step $\Delta t = 0.001$. For comparison purposes, we also present the LO, HO, and BP results. The profiles of numerical solutions along the middle line $\{y = 0.5\}$ are plotted in Figure 4b.

As expected, the results obtained with the entropy stable and bound-preserving LO scheme are free from spurious oscillations and capture the shock location correctly. The HO scheme is neither entropy stable nor bound preserving. In this example, it produces some oscillations around the shock. It is worth noting that these oscillations are less significant than those observed in simulations with classical CG- \mathbb{Q}_1 methods (cf. Figure 2 in [47]). The stabilizing effect of the EG enrichment δu_h was also observed in [33] in the context of linear advection problems.

7.3. Example 3. Convergence test for the two-dimensional KPP problem

In the third example, we consider a smooth version of the two-dimensional Kurganov-Petrova-Popov (KPP) test [48]. The nonlinear hyperbolic conservation law

$$\frac{\partial u}{\partial t} + \nabla \cdot \mathbf{f}(u) = 0, \quad \mathbf{f}(u) = (\sin(u), \cos(u)) \quad (56)$$

is solved in the computational domain $\Omega = (-2, 2) \times (-2.5, 1.5)$. In our grid convergence study, we use the smooth initial condition

$$u_0(x, y) = \begin{cases} \frac{\pi}{4} \left(1 + \frac{1}{20} (1 + \cos(\pi \sqrt{x^2 + y^2}))\right) & \text{if } \sqrt{x^2 + y^2} \leq 1, \\ \frac{\pi}{4} & \text{otherwise.} \end{cases} \quad (57)$$

We select the square entropy $\eta(u) = u^2/2$, which is associated with the entropy flux [44]

$$\mathbf{q}(u) = (\cos(u) + u \sin(u), -\sin(u) + u \cos(u)). \quad (58)$$

When it comes to calculating the artificial viscosity coefficients d_{ij}^e and the LLF fluxes using formulas (35) and (10), respectively, we use $\lambda = 1$ as a global upper bound for the maximum wave speed. More accurate estimates of that speed can be found in [46].

In this test, no analytical solution is available. Therefore, the experimental order of convergence (EOC) for $h = 2^{-7}$ is determined by the differences in the L^1 - and L^2 -norms of numerical solutions on three successively refined grids. Given the numerical solutions calculated on meshes with spacings h , $2h$, and $4h$, the three-level EOCs are calculated as follows:

$$\text{EOC}_{L^1} = \log_2 \left(\frac{\|u_{4h} - u_{2h}\|_{L^1}}{\|u_{2h} - u_h\|_{L^1}} \right), \quad \text{EOC}_{L^2} = \log_2 \left(\frac{\|u_{4h} - u_{2h}\|_{L^2}}{\|u_{2h} - u_h\|_{L^2}} \right).$$

The time step is set to keep the ratio $\Delta t/h = 0.256$ fixed. The values of EOC_{L^1} and EOC_{L^2} are output at the final time $T = 1.0$. Table 1 presents the results of our grid convergence study. It can be seen that the convergence rates of the HO, BP and BP-ES schemes are approximately twice as high as the EOC of the LO approximation.

	LO	HO	BP	BP-ES
EOC_{L^1}	0.87	1.93	1.85	1.82
EOC_{L^2}	0.83	1.73	1.72	1.69

Table 1: Example 3: KPP convergence test with smooth initial conditions, L^1 and L^2 convergence rates.

7.4. Example 4. Two-dimensional rotational KPP test

In the final example, we solve the nonlinear conservation law 56 in the same computational domain, $\Omega = (-2, 2) \times (-2.5, 1.5)$, but using the discontinuous initial condition [48]

$$u_0(x, y) = \begin{cases} \frac{7\pi}{2} & \text{if } \sqrt{x^2 + y^2} \leq 1, \\ \frac{\pi}{4} & \text{otherwise.} \end{cases} \quad (59)$$

The so-defined classical KPP problem admits infinitely many weak solutions. The unique entropy solution at the final time $T = 1.0$ exhibits a two-dimensional rotational wave structure [46, 48, 44]. The challenge of this test is to ensure that a numerical scheme provides entropy stability to prevent convergence to incorrect weak solutions. In our BP-ES method, we perform algebraic entropy fixes using the square entropy $\eta(u) = u^2/2$ and the entropy flux $\mathbf{q}(u)$ given by (58).

We run computations on a uniform mesh using the discretization parameters $h = 2^{-7}$ and $\Delta t = 0.001$. All the other settings are the same as in the Example 3.

In Figures 5 and 6, we compare the EG solutions produced by the LO, BP, and BP-ES schemes at the final time. In addition, we present the BP-ES result obtained using a flux-corrected transport (FCT) algorithm from [33] instead of MCL to enforce preservation of local bounds. Details of the FCT limiting procedure can be found in [23, 33, 34, 42].

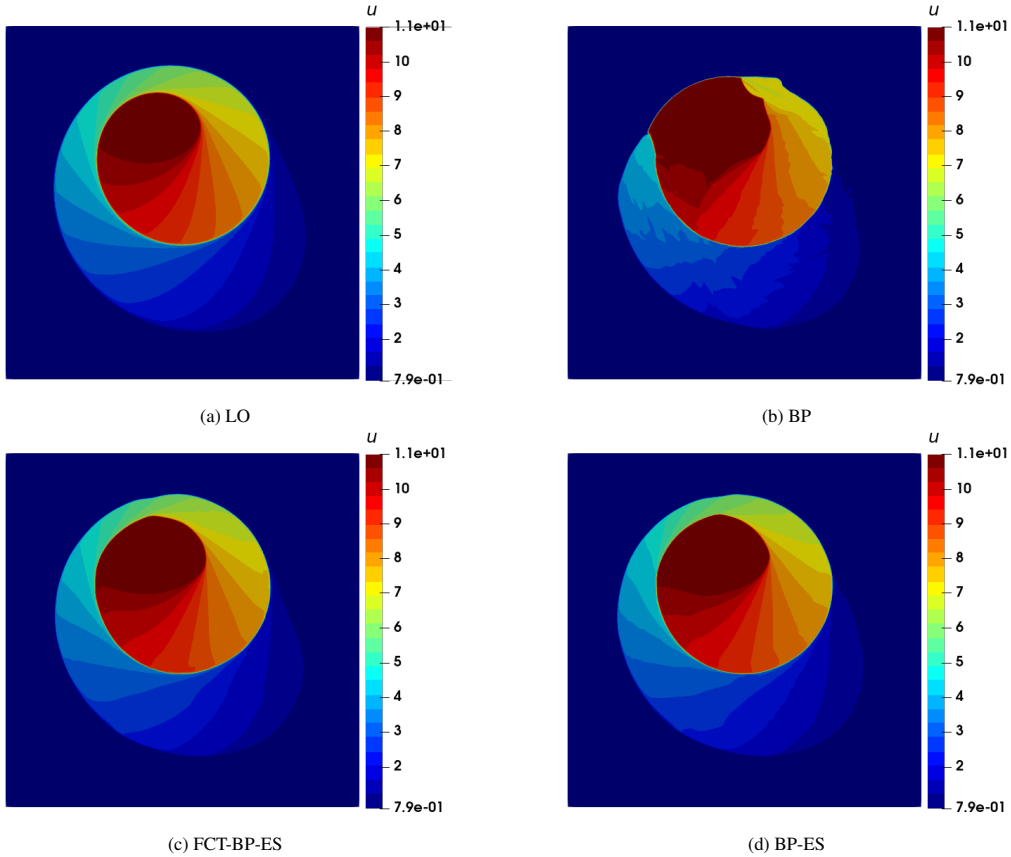
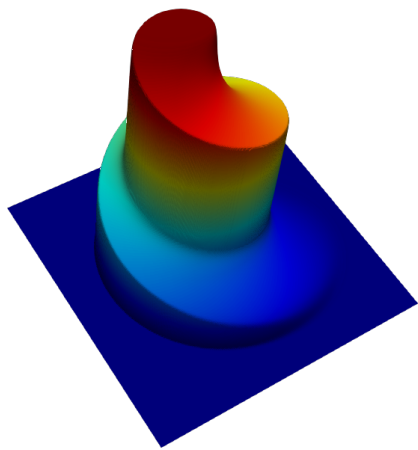
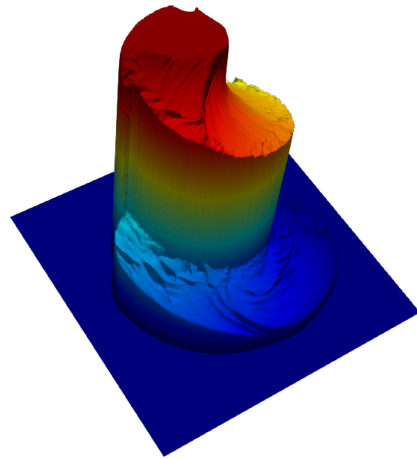


Figure 5: Example 4. Numerical solutions produced by different schemes at $T = 1.0$. The colormap of the filled contour plots represents 25 discrete values in the range $[\frac{7}{4}, \frac{7^2}{2}]$.

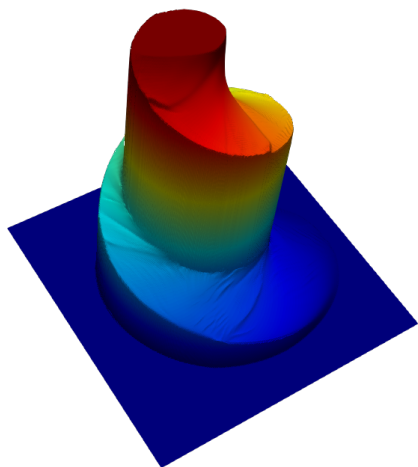
Since the LO scheme is entropy stable, the corresponding numerical solution provides an inaccurate but qualitatively correct approximation to the spiral-shaped shock, as shown in Figure 5a. No entropy stability conditions are enforced in the BP method. As a result, we observe the merging of two shocks in Figure 5b. This failure to reproduce the wave structure of the entropy solution highlights the need to apply entropy fixes. Figures 5c and 5d show that solutions produced by the entropy-stable FCT-BP-ES and BP-ES schemes preserve the correct rotating wave structure, similarly to the LO scheme. For a better visual comparison of the LO, BP-ES, and FCT-BP-ES results, we plot the corresponding solution profiles along the line connecting the top left corner of Ω to the bottom right corner. The plots are displayed in Figure 7.



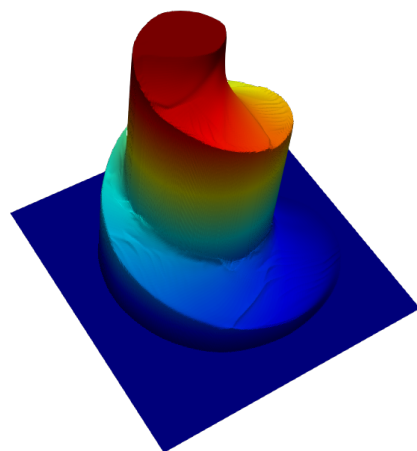
(a) LO



(b) BP



(c) FCT-BP-ES



(d) BP-ES

Figure 6: Example 4: Numerical solutions produced by different schemes at $T = 1.0$.

8. Conclusions

The local conservation property of enriched Galerkin methods makes them a promising tool for solving hyperbolic conservation laws. In the nonlinear case, preservation of local bounds and

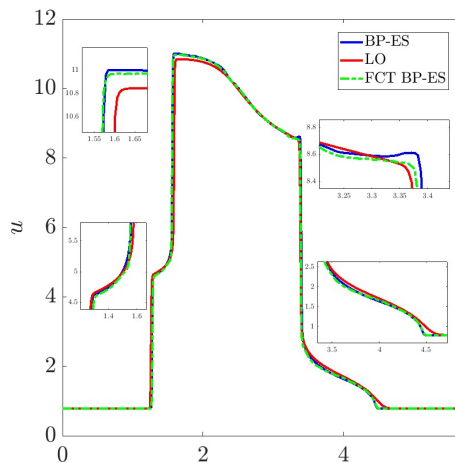


Figure 7: Example 4. Solution profiles along the left diagonal of Ω at $T = 1.0$.

entropy stability are essential requirements for physical admissibility of finite element approximations. The proposed limiting algorithms guarantee the validity of corresponding inequality constraints and preserve optimal convergence behavior in tests with smooth exact solutions. The use of EG cell averages and CG nodal values as degrees of freedom facilitates extensions of modern limiting techniques for finite volume, DG, and CG discretizations of nonlinear hyperbolic systems, such as the Euler equations of gas dynamics and the shallow water equations [23]. The design of customized limiters for EG discretizations of porous media flow models [26, 27, 29] requires more significant effort and represents a prospective avenue for further research.

Acknowledgments

The work of D.K. was supported by the German Research Foundation (DFG) within the framework of the priority research program SPP 2410 under grant KU 1530/30-1. This work for S. L. and Y. Y. are supported by the National Science Foundation under Grant DMS-2208402. The authors thank Insa Schneider (TU Dortmund University) for preliminary numerical studies of the unlimited EG method in one space dimension.

References

- [1] J. Bear, A. Cheng, Modeling Groundwater Flow and Contaminant Transport, Vol. 23, Springer Netherlands, 2010.
- [2] V. Aizinger, C. Dawson, A discontinuous galerkin method for two-dimensional flow and transport in shallow water, *Advances in Water Resources* 25 (1) (2002) 67–84.
- [3] A. A. Khan, W. Lai, Modeling shallow water flows using the discontinuous Galerkin method, CRC Press, 2014.
- [4] R. E. Ewing, Finite element methods for nonlinear flows in porous media, *Computer Methods in Applied Mechanics and Engineering* 51 (1) (1985) 421–439.
- [5] D. W. Peaceman, Fundamentals of numerical reservoir simulation / Donald W. Peaceman, Elsevier Scientific Pub. Co. : distributors for the U.S. and Canada, Elsevier North-Holland Amsterdam ; New York, 1977.
- [6] M. E. Wheeler (Ed.), Numerical Simulation in Oil Recovery, The IMA Volumes in Mathematics and its Applications, Springer-Verlag, 1988.

- [7] J. Bear, A. H.-D. Cheng, Modeling groundwater flow and contaminant transport, Vol. 23, Springer, 2010.
- [8] G. P. Karatzas, Developments on modeling of groundwater flow and contaminant transport, *Water Resources Management* 31 (2017) 3235–3244.
- [9] G. R. Barrenechea, V. John, P. Knobloch, Analysis of algebraic flux correction schemes, *SIAM Journal on Numerical Analysis* 54 (4) (2016) 2427–2451.
- [10] D. Kuzmin, Algebraic flux correction I. Scalar conservation laws, in: D. Kuzmin, R. Löhner, S. Turek (Eds.), *Flux-Corrected Transport: Principles, Algorithms, and Applications*, 2nd Edition, Springer, 2012, pp. 145–192.
- [11] D. Kuzmin, M. Möller, M. Garris, Algebraic flux correction II. Compressible flow problems, in: D. Kuzmin, R. Löhner, S. Turek (Eds.), *Flux-Corrected Transport: Principles, Algorithms, and Applications*, 2nd Edition, Springer, 2012, pp. 193–238.
- [12] D. Kuzmin, M. Möller, J. N. Shadid, M. Shashkov, Failsafe flux limiting and constrained data projections for equations of gas dynamics, *Journal of Computational Physics* 229 (23) (2010) 8766–8779.
- [13] R. Löhner, K. Morgan, J. Peraire, M. Vahdati, Finite element flux-corrected transport (FEM-FCT) for the Euler and Navier–Stokes equations, *International Journal for Numerical Methods in Fluids* 7 (10) (1987) 1093–1109.
- [14] C. Lohmann, D. Kuzmin, Synchronized flux limiting for gas dynamics variables, *Journal of Computational Physics* 326 (2016) 973–990.
- [15] S. T. Zalesak, Fully multidimensional flux-corrected transport algorithms for fluids, *Journal of Computational Physics* 31 (3) (1979) 335–362.
- [16] C. J. Cotter, D. Kuzmin, Embedded discontinuous Galerkin transport schemes with localised limiters, *Journal of Computational Physics* 311 (2016) 363–373.
- [17] C. Lohmann, D. Kuzmin, J. N. Shadid, S. Mabuza, Flux-corrected transport algorithms for continuous Galerkin methods based on high order Bernstein finite elements, *Journal of Computational Physics* 344 (2017) 151–186.
- [18] J.-L. Guermond, M. Nazarov, B. Popov, I. Tomas, Second-order invariant domain preserving approximation of the Euler equations using convex limiting, *SIAM Journal on Scientific Computing* 40 (5) (2018) A3211–A3239.
- [19] D. Kuzmin, Monolithic convex limiting for continuous finite element discretizations of hyperbolic conservation laws, *Computer Methods in Applied Mechanics and Engineering* 361 (2020) 112804.
- [20] D. Kuzmin, H. Hajduk, A. Rupp, Limiter-based entropy stabilization of semi-discrete and fully discrete schemes for nonlinear hyperbolic problems, *Computer Methods in Applied Mechanics and Engineering* 389 (2022) 114428.
- [21] D. Kuzmin, M. Quezada de Luna, Algebraic entropy fixes and convex limiting for continuous finite element discretizations of scalar hyperbolic conservation laws, *Computer Methods in Applied Mechanics and Engineering* 372 (2020) 113370.
- [22] E. Tadmor, Entropy stability theory for difference approximations of nonlinear conservation laws and related time-dependent problems, *Acta Numerica* 12 (2003) 451–512.
- [23] D. Kuzmin, H. Hajduk, *Property-Preserving Numerical Schemes for Conservation Laws*, World Scientific, 2023.
- [24] R. Becker, E. Burman, P. Hansbo, M. G. Larson, A reduced p^1 -discontinuous Galerkin method, *Chalmers Finite Element Center Preprint 2003-13*, Chalmers University of Technology (2003).
- [25] S. Sun, J. Liu, A locally conservative finite element method based on piecewise constant enrichment of the continuous galerkin method, *SIAM Journal on Scientific Computing* 31 (4) (2009) 2528–2548.
- [26] S. Lee, Y.-J. Lee, M. F. Wheeler, A locally conservative enriched Galerkin approximation and efficient solver for elliptic and parabolic problems, *SIAM Journal on Scientific Computing* 38 (3) (2016) A1404–A1429.
- [27] S. Lee, M. F. Wheeler, Adaptive enriched Galerkin methods for miscible displacement problems with entropy residual stabilization, *Journal of Computational Physics* 331 (2017) 19–37.
- [28] R. Juanes, T. W. Patzek, Multiscale-stabilized solutions to one-dimensional systems of conservation laws, *Computer methods in Applied Mechanics and Engineering* 194 (25-26) (2005) 2781–2805.
- [29] S. Lee, M. F. Wheeler, Enriched Galerkin methods for two-phase flow in porous media with capillary pressure, *Journal of Computational Physics* 367 (2018) 65–86.
- [30] J. Choo, S. Lee, Enriched galerkin finite elements for coupled poromechanics with local mass conservation, *Computer Methods in Applied Mechanics and Engineering* 341 (2018) 311–332.
- [31] S. Lee, S.-Y. Yi, Locking-free and locally-conservative enriched Galerkin method for poroelasticity, *Journal of Scientific Computing* 94 (1) (2023) 26.
- [32] S.-Y. Yi, S. Lee, Physics-preserving enriched galerkin method for a fully-coupled thermo-poroelasticity model, *Numerische Mathematik* (2024) 1–30.
- [33] D. Kuzmin, H. Hajduk, A. Rupp, Locally bound-preserving enriched Galerkin methods for the linear advection equation, *Computers & Fluids* 205 (2020) 104525.
- [34] D. Kuzmin, A new perspective on flux and slope limiting in discontinuous Galerkin methods for hyperbolic conservation laws, *Computer Methods in Applied Mechanics and Engineering* 373 (2021) 113569.
- [35] L. C. Evans, *Partial differential equations*, American Mathematical Society, Providence, R.I., 2010.
- [36] C. Fletcher, The group finite element formulation, *Computer Methods in Applied Mechanics and Engineering* 37 (2) (1983) 225–244.

- [37] V. Selmin, L. Formaggia, Unified construction of finite element and finite volume discretizations for compressible flows, *International Journal for Numerical Methods in Engineering* 39 (1) (1996) 1–32.
- [38] D. Kuzmin, M. Quezada de Luna, Entropy conservation property and entropy stabilization of high-order continuous Galerkin approximations to scalar conservation laws, *Computers & Fluids* 213 (2020) 104742.
- [39] A. Jameson, Computational algorithms for aerodynamic analysis and design, *Applied Numerical Mathematics* 13 (5) (1993) 383–422.
- [40] A. Jameson, Positive schemes and shock modelling for compressible flows, *International Journal for Numerical Methods in Fluids* 20 (8–9) (1995) 743–776.
- [41] D. Kuzmin, M. Quezada de Luna, D. I. Ketcheson, J. Gröll, Bound-preserving convex limiting for high-order Runge–Kutta time discretizations of hyperbolic conservation laws, *Journal of Scientific Computing* 91 (2022) 21.
- [42] D. Kuzmin, Entropy stabilization and property-preserving limiters for \mathbb{P}_1 discontinuous galerkin discretizations of scalar hyperbolic problems, *Journal of Numerical Mathematics* 29 (4) (2021) 307–322.
- [43] D. Arndt, W. Bangerth, M. Feder, M. Fehling, R. Gassmöller, T. Heister, L. Heltai, M. Kronbichler, M. Maier, P. Munch, J.-P. Pelteret, S. Sticko, B. Turcksin, D. Wells, The deal.II library, version 9.4, *Journal of Numerical Mathematics* Accepted (2022).
- [44] D. Kuzmin, H. Hajduk, A. Rupp, Limiter-based entropy stabilization of semi-discrete and fully discrete schemes for nonlinear hyperbolic problems, *Computer Methods in Applied Mechanics and Engineering* 389 (2022) 114428.
- [45] J.-L. Guermond, B. Popov, Invariant domains and first-order continuous finite element approximation for hyperbolic systems, *SIAM Journal on Numerical Analysis* 54 (4) (2016) 2466–2489.
- [46] J.-L. Guermond, B. Popov, Invariant domains and second-order continuous finite element approximation for scalar conservation equations, *SIAM Journal on Numerical Analysis* 55 (6) (2017) 3120–3146.
- [47] D. Kuzmin, J. Vedral, Dissipation-based weno stabilization of high-order finite element methods for scalar conservation laws, *Journal of Computational Physics* 487 (2023) 112153.
- [48] A. Kurganov, G. Petrova, B. Popov, Adaptive semidiscrete central-upwind schemes for nonconvex hyperbolic conservation laws, *SIAM Journal on Scientific Computing* 29 (6) (2007) 2381–2401.